Journal of Materials Processing Technology 241 (2017) 24–35

Contents lists available at ScienceDirect

Journal of Materials Processing Technology

journal homepage: www.elsevier.com/locate/jmatprotec

Laser spot welding of laser textured steel to aluminium

Goncalo Pardal[a,*], Sonia Meco[a], Andrew Dunn[b,c], Stewart Williams[a], Supriyo Ganguly[a], Duncan P. Hand[b], Krystian L. Wlodarczyk[b]

[a] Welding Engineering and Laser Processing Centre, Cranfield University, Cranfield, Bedfordshire, MK43 0AL, United Kingdom
[b] Institute of Photonics and Quantum Sciences, School of Engineering and Physical Sciences, Heriot-Watt University, Edinburgh, EH11 4AS, United Kingdom
[c] SPI Lasers UK Ltd, Cosford Lane, Swift Valley Industrial Estate, Rugby, CV21 1QN, United Kingdom

ARTICLE INFO

Article history:
Received 9 May 2016
Received in revised form
23 September 2016
Accepted 31 October 2016
Available online 2 November 2016

Keywords:
Laser processing
Laser texturing
Laser spot welding
Surface modification
Dissimilar metals

ABSTRACT

Laser welding of dissimilar metals (steel and aluminium) was investigated with the aim to increase the maximum tensile shear load of the Fe-Al joints. The increase was achieved by texturing the surface of steel prior to the laser spot welding process which was performed in a lap-joint configuration with the steel positioned on top of the aluminium and with a texture faced down to the aluminium surface. This configuration enabled an increase of the bonding area of the joints, because the molten aluminium filled in the gaps of the texture, without the need of increasing the process energy which typically leads to the growth of the intermetallic compounds. Different textures (containing hexagonally arranged craters, parallel lines, grid and spiral patterns) were tested with different laser welding parameters. The Fe-Al joints obtained with the textured steel were found to have up to 25% higher maximum tensile-shear load than the joints obtained with the untextured steel.

1. Introduction

One of the challenges in the automotive industry is to reduce the carbon emission of manufactured vehicles (Church, 2015; Havrilla, 2014; Lesemann et al., 2008). This can be done by incorporating lightweight metallic alloys, such as aluminium alloys, with more generic automotive modulus often made of uncoated mild steel in order to reduce the total mass of a vehicle. Unfortunately, joining these two dissimilar metals is difficult due to the chemical reactions between aluminium and steel that lead to the formation of intermetallic compounds (IMC) at the metals' interface during the welding process and thus the mechanical properties of the welds are deteriorated (Martinsen et al., 2015).

A thin sheet of steel (DC04 grade) can be successfully welded to an aluminium alloy (6111-T4) using a conduction mode laser spot welding process (Pardal et al., 2014). This novel welding technique relies on the incidence of a defocused laser beam on the top surface of steel and the generation of heat resultant from the laser-material interaction that is conducted to the aluminium through the steel. In this process the welding parameters need to be controlled in order to melt only the aluminium at the interface. The backing bar underneath the Al alloy is used to facilitate the heat extraction and minimise the IMC growth (Borrisutthekul et al., 2007). This technique differs from regular laser welding because here only aluminium is melted whilst steel remains in solid state. Although this approach helps to minimise the mixing of Al with Fe, due to a maximum solubility of 12% Al in Fe, a thin IMC layer is still produced which leads to a reduction in weld strength. As reported by (Pardal et al., 2014), the thickness of the IMC layer depends on the temperature profile generated by the laser spot and the heat distribution across the interface. However, the thermal field is also responsible for geometry of the fusion zone of the aluminium and thus the dimension of the bonding area. Previous results reported by (Meco et al., 2015) suggest that when a larger bonding area is created the joints have higher maximum shear load. One would expect a linear evolution of the tensile-shear load of dissimilar metal joints with the bonding area. However, this trend is not observed in dissimilar metal joining because the IMC layer becomes thicker simultaneously with the growth of the bonding area.

Resistance spot welding (RSW) can also be used for joining thin sheets of steel to an aluminium alloy, as demonstrated by (Zhang et al., 2011) and (Qiu et al., 2009a,b). The first of these papers reported welding of a 1 mm thick galvanized high strength steel to 1.5 mm thick 6008 aluminium alloy and obtained the Fe-Al joints with the maximum tensile-shear load of 3.3 kN. By correlating the mechanical strength of the joints with the process parameters, it

* Corresponding author.
E-mail address: g.n.rodriguespardal@cranfield.ac.uk (G. Pardal).

http://dx.doi.org/10.1016/j.jmatprotec.2016.10.025

Table 1
Chemical composition in weight% of Al 5083 and CR4 steel according to the standards BS EN 573-3:2009 and EN10130-2006, respectively.

Element	Al	Fe	Mn	Ti	Mg	Cu	Si	Zn	Cr	C	P	Other
Al 5083	Bal.	0.4 max	0.4–1.0	0.05–0.25	4.0–4.9	0.1 max	0.0–0.4	0.0–0.1	0.05–0.25	–	–	0.0–0.15
CR4	–	Bal.	0.6 max	–	–	–	–	–	–	0.12 max	0.045 max	

was found that the tensile-shear load of the joints increased with the increasing welding current and time. Detailed examination of the joints provided evidence that the increase of the process parameters leads to the increase of the weld nugget diameter as well as to the growth of IMC. The second of these papers (Qiu et al., 2009a,b) described use of the RSW process with a cover plate to join 1 mm thick SPCC steel to 1 mm thick 5052 aluminium alloy. This welding approach enabled the generation of the Fe-Al joints with the maximum tensile-shear load of approximately 5 kN. Although the authors confirmed that the tensile-shear load increases with the increasing weld nugget diameter, they also provided evidence that the presence of the IMC layer reduces the maximum load of the dissimilar Fe-Al joints compared to the Al–Al joints. Under similar welding conditions, the maximum tensile-shear load of the Al–Al joints was about 6 kN, and hence a 1 kN higher than that obtained with the Fe-Al joints. The use of metallic inserts was also investigated in RSW for joining 0.8 mm thick low carbon steel to 1 mm thick 5XXX series aluminium alloy (Oikawa and Saitoh, 1999). The insert metal sheets were aluminium clad steel sheets manufactured by hot rolling with a direct resistance heating process. These inserts were positioned between the steel and the aluminium sheets with the steel side of the insert facing the steel and the aluminium side of the insert facing the aluminium sheet. This metallic combination was found to be stronger than that without the metallic insert (3.3 kN compared to 2 kN).

An alternative approach to join thin sheets of galvanized steel to 6061 aluminium alloy by spot welding has been investigated using a variant of arc welding process called Cold Metal Transfer, also known as CMT (Cao et al., 2014). In this study, 4043 aluminium wire was used to create a spot plug by filling in a hole previously machined on the metallic sheet which was positioned on the top of the lap-joint. The material stacking configuration and welding variables were investigated in terms of microstructure and mechanical strength. The authors found that when the steel was positioned on the top there was no presence of IMCs in the middle on the surface of the fractured joint. On the other hand, when aluminium was positioned on the top, the molten aluminium was deposited onto the steel surface and the reaction between Fe and Al occurred, forming $FeAl_3$ and Fe_2Al_5 at the joint interface. The fracture load of the joints with the aluminium on the top was about 5 kN which was higher than when the steel was on the top or even when the joint was produced between the coupons of aluminium (3 kN). The reason for these results was the nugget diameter that in the steel-aluminium joint was smaller than that in the aluminium-steel joint configuration.

A modified friction stir spot welding (FSSW), called abrasion circle FSSW was used by (Chen et al., 2012) to join 6111-T4 aluminium alloy to DC04 low carbon steel. The authors showed that IMCs were not formed on the joint and the maximum tensile-shear load registered was near 4 kN. The abrasion circle FSSW enabled the increase of the bonding area by translating the tool through an orbital path.

In this paper, an alternative spot welding approach to increase the bonding area between steel and aluminium alloy without modifying the laser-generated temperature profile is proposed and investigated. A nanosecond pulsed laser is used for texturing the surface of steel prior to laser spot welding in order to locally increase the bonding area between these two dissimilar metals. The aim of this work is to investigate the impact of various laser-generated textures on the mechanical properties (strength) of the Fe-Al welds as well as to understand the mechanism of their formation.

Table 2
Mechanical strength of Al 5083 and CR4 steel.

	Ultimate tensile strength, MPa	Yield strength, MPa	Hardness, HV
Al 5083	275–350	125 min	87
CR4	270–410	280 max	105

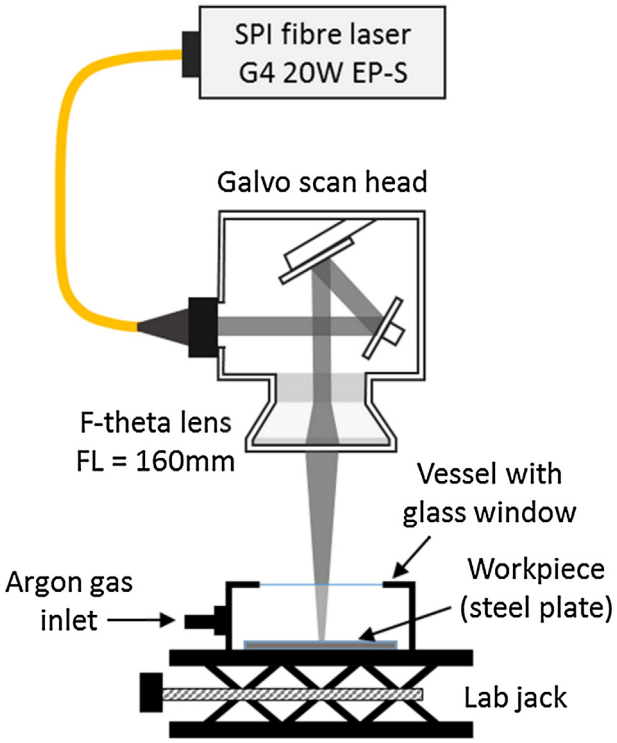

Fig 1. Schematic of the laser system used for texturing the surface of steel.

2. Experimental procedure

2.1. Material

A 1 mm thick 5083 aluminium alloy and 0.85 mm thick CR4 grade mild steel were used in the experiments. The steel and aluminium coupons were 100 mm long and 40 mm wide. Tables 1 and 2 show the chemical composition and the mechanical properties of these two metals.

2.2. Laser texturing of steel

2.2.1. Methodology and experimental setup

Fig. 1 shows a schematic of the laser machining system used for texturing the steel coupons. The laser source was a pulsed SPI 20 W fibre laser (G4 EP-S) that provided 220 ns long pulses (full width 10% maximum) with a pulse repetition frequency of 28 kHz, wavelength of 1064 nm and maximum pulse energy of 0.71 mJ. The low cost, high flexibility and acceptable absorption of this wavelength make

Fig. 2. Steel coupons with the laser-generated textures containing 30 μm deep parallel troughs (left) and a 30 μm deep spiral trough (right).

this type of laser well suited for texturing the surface of steel (Dunn et al., 2015, 2014; Vilhena et al., 2009). The laser beam was delivered to the work piece via a galvoscanner equipped with a 160 mm focal length F-theta lens. The galvoscanner was controlled by a PC using SCAPS Samlight software. The nominal spot diameter on the work piece was 22 μm ($1/e^2$ of its maximum intensity, $M^2 \sim 1.1$).

Prior to laser texturing, both surfaces of the steel coupons were cleaned with acetone to remove oil and debris. Later, the work piece was placed in a metal vessel (enclosure) containing a glass window. This vessel allowed the steel coupons to be machined under low-pressure argon gas in order to avoid oxidation of the steel, which could have an impact on the quality of welds.

Prior to texturing a large quantity of the steel coupons, the laser-induced craters were characterized for various laser processing settings, in particular pulse energy (E_P) and number of laser pulses (N). The diameter and depth of these craters were measured using an optical microscope (Leica DM6000 M) and a 3D surface profilometer (InfiniteFocus® Alicona). Following the calibration process, seven different test textures were generated on the surface of the steel coupons. The area selected for texturing was either a 40 mm by 40 mm square or a 40 mm diameter circle, as shown in Fig. 2, depending on the texture pattern. Each texture was produced on at least 12 coupons, providing a relatively large number of samples for testing various settings for laser spot welding, in particular average power (P_A) and interaction (irradiation) time.

2.2.2. Calibration

Individual craters were generated on the surface of CR4 mild steel by varying the pulse energy (E_P) between 0.04 mJ and 0.71 mJ and varying the number of laser pulses (N) per spot between 1 and 10, by repeatedly passing the laser beam over the work piece. The depth of craters obtained for various values of E_P and N is shown in Fig. 3. The error bars plotted on these graphs are the standard deviations of three separate measurements for the craters generated with the constant pulse energy and number of laser pulses.

Fig. 3a) reveals that the depth of the craters increases significantly and almost linearly with increasing number of laser pulses. This means that each laser pulse (with energy above the ablation threshold, 0.04 mJ) removes approximately the same depth of material from the laser-irradiated area. Fig. 3b, in turn, shows that the depth of the craters increases insignificantly with increasing pulse energy, in particular for a low number of laser pulses.

The diameter of the craters was also measured and the results are presented in Fig. 4. They show the crater diameter is almost unchanged for the increasing number of laser pulses, in particular

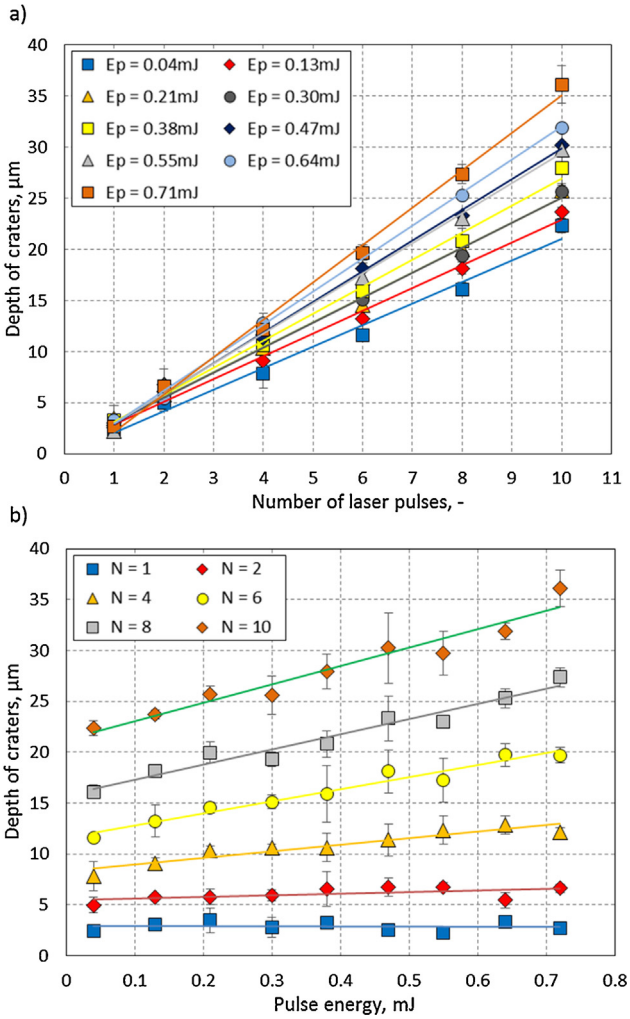

Fig. 3. Depth of craters as a function of: a) number of laser pulses for different pulse energies, b) pulse energy for different number of laser pulses. Solid lines are trend lines.

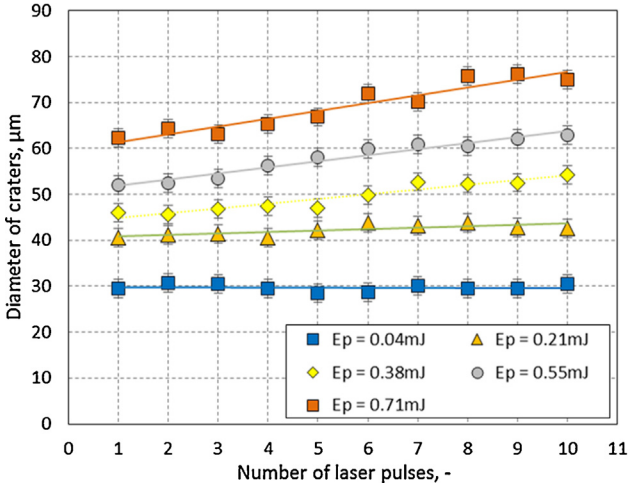

Fig. 4. Diameter of craters as a function of number of laser pulses for different pulse energies. Solid lines are trend lines.

Table 3
List of laser processing parameters used for the generation of various textures on the surface of the steel coupons.

Texture	Pattern	E_P, mJ	Number of pulses	v, mm/s	Processing rate, s/cm^{-2}	D, μm	Φ, μm	S_D, μm
A	Hexagonal	0.55	10	2240	9.5	30	65	80
B	Hexagonal	0.55	10	3500	4.6	30	65	125
C	Hexagonal	0.17	12	3500	5.5	30	40	125
D	Hexagonal	0.17	12	1400	25.7	30	40	50
E	Lines	0.17	5	350	30.6	30	40	50
F	Spiral	0.17	5	350	22.2	30	40	50
G	Grid	0.17	5	350	61.2	30	40	50

for $E_P < 0.21$ mJ. For higher pulse energies, it was observed that the crater diameter increases at a rate of < 1.5 μm per pulse.

In general, the results presented in Figs. 3 and 4 seem to follow the similar trends that were observed in the other types of steel (100Cr6 and grade 304) by Dunn et al. (Dunn et al., 2014) and Vilhena et al. (Vilhena et al., 2009).

2.2.3. Generation of test textures on steel

The results presented in the previous section (Section 2.2.2) show clearly that it is possible to almost independently control both the depth and the diameter of the laser-induced craters on the surface of grade CR4 mild steel. By using the correct pulse energy and the number of laser pulses, the dimension of the craters can hence be tailored and therefore various textures can be generated.

Seven different textures were generated on the surface of the steel coupons. Three dimensional surface profiles of these textures measured with the Alicona instrument are shown in Fig. 5. Four of them comprised of craters that were arranged in a hexagonal pattern (see Textures A–D), each texture having craters with a nominal depth (D) of 30 μm (±5 μm), diameter (Φ) of either 40 μm or 65 μm, and separation distance (S_D) between the craters of either 50 μm, 80 μm or 125 μm. The other three textures contained either parallel troughs (see Texture E), a spiral trough (see Texture F) or a grid of troughs (see Texture G). The troughs in all three textures were approximately 30 μm deep, 40 μm wide and were separated by a fixed distance of 50 μm.

Table 3 provides a list of laser processing parameters (i.e. pulse energy, number of laser pulses, and scan speed) that were used for the generation of the textures shown in Fig. 5. Textures A-D (containing craters arranged in a hexagonal pattern) were generated following the texturing procedure described in (Dunn et al., 2014). Various separation distances between the craters were obtained by modifying the scan speed (v) and hatch distance (h). The hatch distance was calculated using the following formula:

$$h = \frac{\sqrt{3}}{2} \times \frac{v}{PRF} \quad (1)$$

where PRF is the pulse repetition frequency.

The textures E-G (those containing troughs) were generated by moving the laser beam with a speed of 350 mm/s. Since the pulse overlap at this speed was approximately 57%, which corresponds to slightly more than two pulses per laser spot, it was necessary to apply 5 laser passes in order to obtain approximately 30 μm deep troughs (based on the results in Fig. 4).

2.3. Laser welding of textured steel to aluminium

2.3.1. Methodology and experimental setup

All the surfaces of the aluminium and the untextured surface of the steel coupons were cleaned before welding with an abrasive pad and acetone to remove contaminants. The textured surface of the steel was left as processed.

A multi-mode IPG CW fibre laser with a maximum power of 8 kW and a wavelength of 1070 nm was used for welding the laser-textured steel to the aluminium. The welding process was performed using a 13 mm diameter laser beam that was defocused on the untextured side of the steel, as shown in Fig. 6a. The laser-textured surface of the steel was faced down, being in a very close contact with the aluminium coupon. The steel and aluminium coupons were positioned on the clamping system in a lap-joint configuration with an overlap of 35 mm (Fig. 6b) and clamped (Fig. 6c). The ring on the steel applied uniform load on the substrate around the weld and it had three outlets to shield the weld with argon.

Table 4
Laser welding parameters used for Textures A-D (preliminary tests).

D_{beam}, mm	P, kW	t_i, s	PD, MW/m^2	E_{sp}, kJ
13.00	2.00	3.0	15.1	6.0
13.00	2.00	4.0	15.1	8.0
13.00	2.00	5.0	15.1	10.0
13.00	2.00	6.0	15.1	12.0
13.00	2.67	3.0	20.1	8.0
13.00	3.67	3.0	27.6	11.0
13.00	4.00	3.0	30.1	12.0

The laser power and irradiation time were used as variables for welding the laser-textured steel samples to the aluminium coupons. The analysis of the welding results, however, was made using the fundamental laser material interaction parameters, i.e. the power density (PD), interaction time (t_i) and specific point energy (E_{sp}), because these parameters can be used to transfer the welding process between various laser systems (Assuncao et al., 2012; Williams and Suder, 2011). The PD, t_i and E_{sp} values were calculated based on the system parameters, using the following equations:

$$\text{Power density, MW/m}^2 \quad PD = \frac{\text{Power}}{A_{beam}} \quad (2)$$

$$\text{Interaction time, s} \quad t_i = \text{irradiation time} \quad (3)$$

$$\text{Special point energy, } k_j \quad E_{sp} = PD \times t_i \times A_{beam} \quad (4)$$

The specific point energy corresponds to the energy transferred to the material through the laser spot and it is calculated by the product of the power density by the interaction time and the area of the laser beam (A_{beam}). The interaction of the laser with the material induces a thermal field that results in partial melting of the steel. As the heat conducts through the steel and is transferred to the aluminium, the temperature at the joint interface increases and melting of the aluminium occurs. The energy of the welding process must be controlled to avoid the melting of the full thickness of the steel sheet. This process enables the wetting of the steel surface by the molten aluminium reducing the diffusion of Fe in Al.

The laser welding parameters that were used in our preliminary and final welding experiments are listed in Tables 4 and 5, respectively.

2.3.2. Tensile shear test

The mechanical tensile-shear tests were performed using a 100 kN INSTRON 5500R tensile test machine. The experiments were

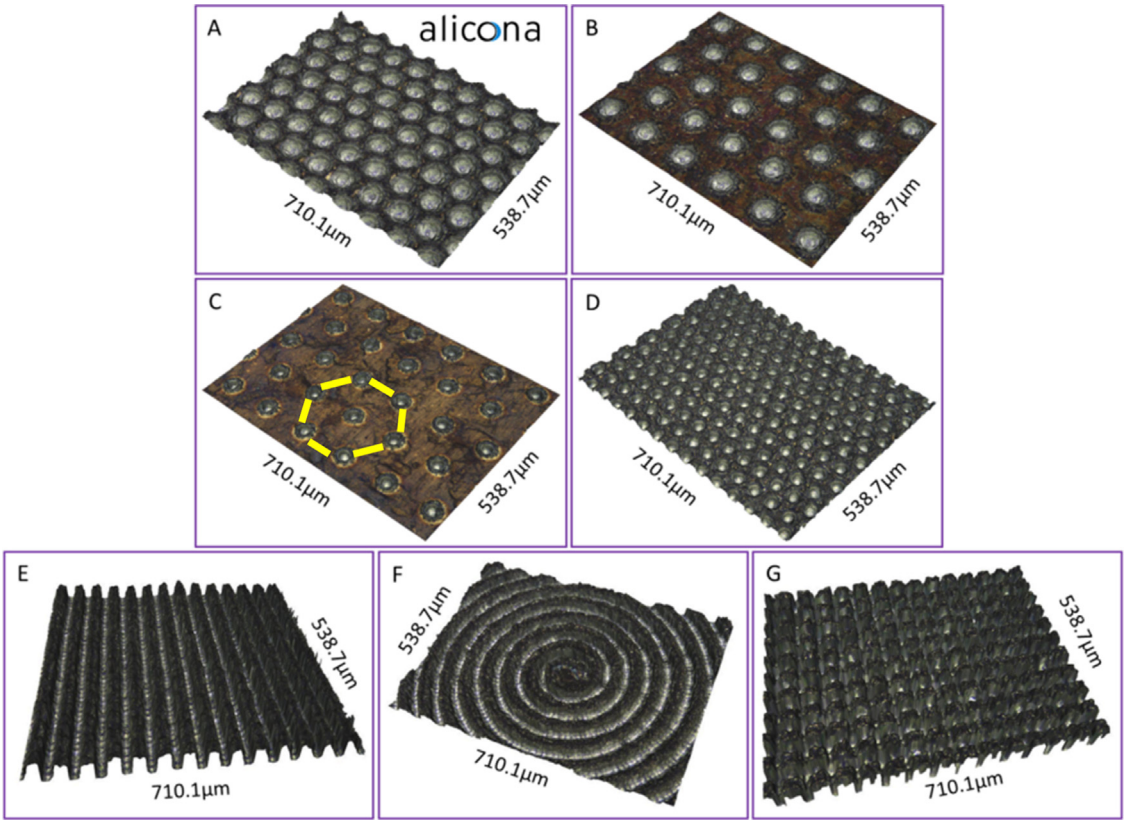

Fig. 5. Test textures generated on the surface of grade CR4 mild steel. Textures A–D contain craters arranged in a hexagonal pattern, texture E contains parallel troughs, texture F contains a spiral trough, and texture G contains a grid of troughs. The surface profiles were obtained with the Alicona instrument.

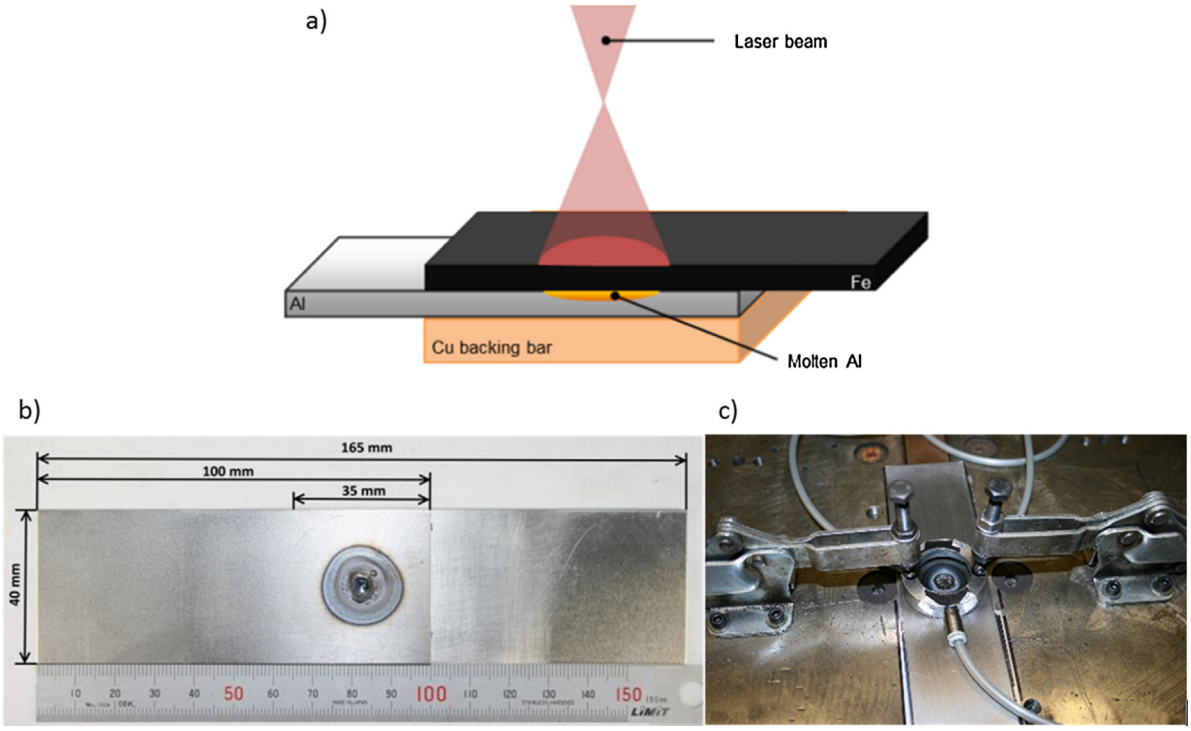

Fig. 6. a) Schematic of the laser spot welding process, b) steel and Al sample dimensions and experimental overlap and c) photograph of the clamping system used for welding steel to aluminium.

carried out with constant cross-head speed of 1 mm/min and at room temperature. The load and displacement were acquired by a National Instruments system connected to a laser extensometer with a gauge length of 50 mm.

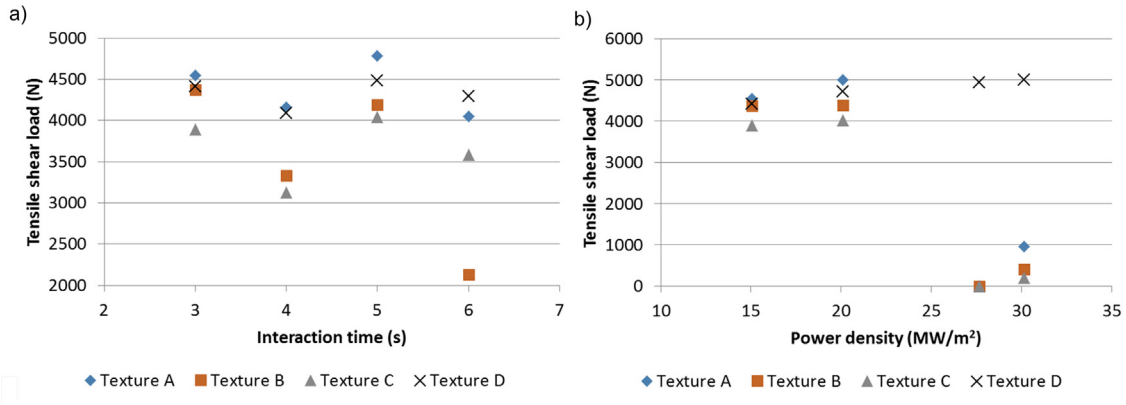

Fig. 7. Tensile shear load obtained with Textures A–D as a function of: a) interaction time (t_i), while PD = 15.1 MW/m^2 and b) power density (PD), while t_i = 3 s.

Table 5
Laser welding parameters used for Textures D-F (final tests).

D_{beam}, mm	P, kW	t_i, s	PD, MW/m^2	E_{sp},kJ
13.00	2.67	3.00	20.1	8.0
13.00	2.67	4.00	20.1	10.7
13.00	2.67	5.00	20.1	13.4
13.00	2.25	3.00	17.0	6.8
13.00	3.00	3.00	22.7	9.0

Table 6
Relative contact area at the Fe-Al interface estimated for Textures A-D.

Texture	A	B	C	D
Relative contact area (S)	42%	73%	90%	44%

3. Results and discussion

3.1. Preliminary tests for hexagonal geometry

A preliminary study was carried out to determine the best texture for laser spot welding in terms of crater depth, diameter and spacing for different welding parameters. The laser welding parameters listed in Table 4 were used and the experimental results are shown in Fig. 7. In this experiment no comparison was made with the untextured samples.

Fig. 7a) shows that Textures A and D always provided higher tensile-shear load of the joints (> 4 kN) than Textures B and C, independently on the interaction time (t_i). Poorer mechanical performance of the joints with Textures B and C may be related to the large spacing between craters, which in these two textures was 125 μm compared to 80 and 50 μm for Textures A and D, respectively. To better illustrate this, the relative contact area (S) of each texture was calculated and the results are in Table 6. The S values were calculated as follows:

$$S = \frac{ContactArea}{TotalArea}.100\% \quad (5)$$

where Contact Area is the white area shown in Fig. 8 (expressed in mm^2 units), whereas Total Area is equal to 0.25 mm^2 (500 μm × 500 μm).

A large spacing between craters (as in Textures B and C) represents a smaller surface area available on the steel for the molten aluminium to flow and create the bonding between both metals. The results in Fig. 8 suggest that the interaction time (between 3 and 6 s) does not significantly affect the maximum tensile shear load of the joints. There was only one point (obtained with Texture B and t_i = 6 s) which provided a tensile shear load of < 3 kN. In general, the results indicate that a texture with smaller spacing between craters and smaller contact area should be used to improve maximum shear load of the joint.

Table 7
Relative contact area at the Fe-Al interface estimated for Textures E-G.

	Texture E (Lines)	Texture F (Spiral)	Texture G (Grid)
Relative contact area (S)	20%	23%	4%

A similar trend was observed for the joints produced with the different power density (Fig. 7b). For any value of power density, Textures B and C seem to have lower maximum tensile shear load when compared to Textures A and D. There is also a difference in the mechanical performance of the joints produced with Textures A and D. The joints produced with Texture D were the only ones in which the tensile shear load did not deteriorate with the increase of the power density. All the other textures had considerably reduced the tensile shear load of the joints for power density values above 25 MW/m^2. This shows that not only the spacing between craters is important but also the crater diameter needs to be controlled to obtain the maximum tensile shear load for a wide range of laser welding parameters.

3.2. Results for several geometric patterns

In the present section, the characteristics of Texture D were used for the generation of different patterns on the steel surface, viz. grid, lines, and spiral. The performance of the new textures was tested for different levels of the specific point energy by varying the power density and the interaction time. The aim was to investigate how the textures with different geometrical patterns affect the mechanical strength and the wetting area of the joints, and compare these features against the untextured samples.

The contact area between the steel and the aluminium varies with the pattern due to their different geometrical designs. Fig. 9 illustrates how the laser-generated patterns affect the contact area at the metals interface, whereas Table 7 provides the values of the relative contact area that were estimated for these three textures. The texture with the smallest contact area is the grid pattern (S = 4%). The line and spiral patterns were found to have similar contact areas (S = 20%).

The tensile shear load of the joints produced with the new geometric patterns was evaluated against the untextured samples (see Fig. 10). The joints were produced with constant power density of 20.1 MW/m^2 and variable interaction time. Fig. 10 shows that the spiral texture did not generate good joints when the interaction time (t_i) was 4 s. The joint generated with t_i = 4 s had a tensile shear load of < 1 kN, whereas the joint with t_i = 5 s was not produced.

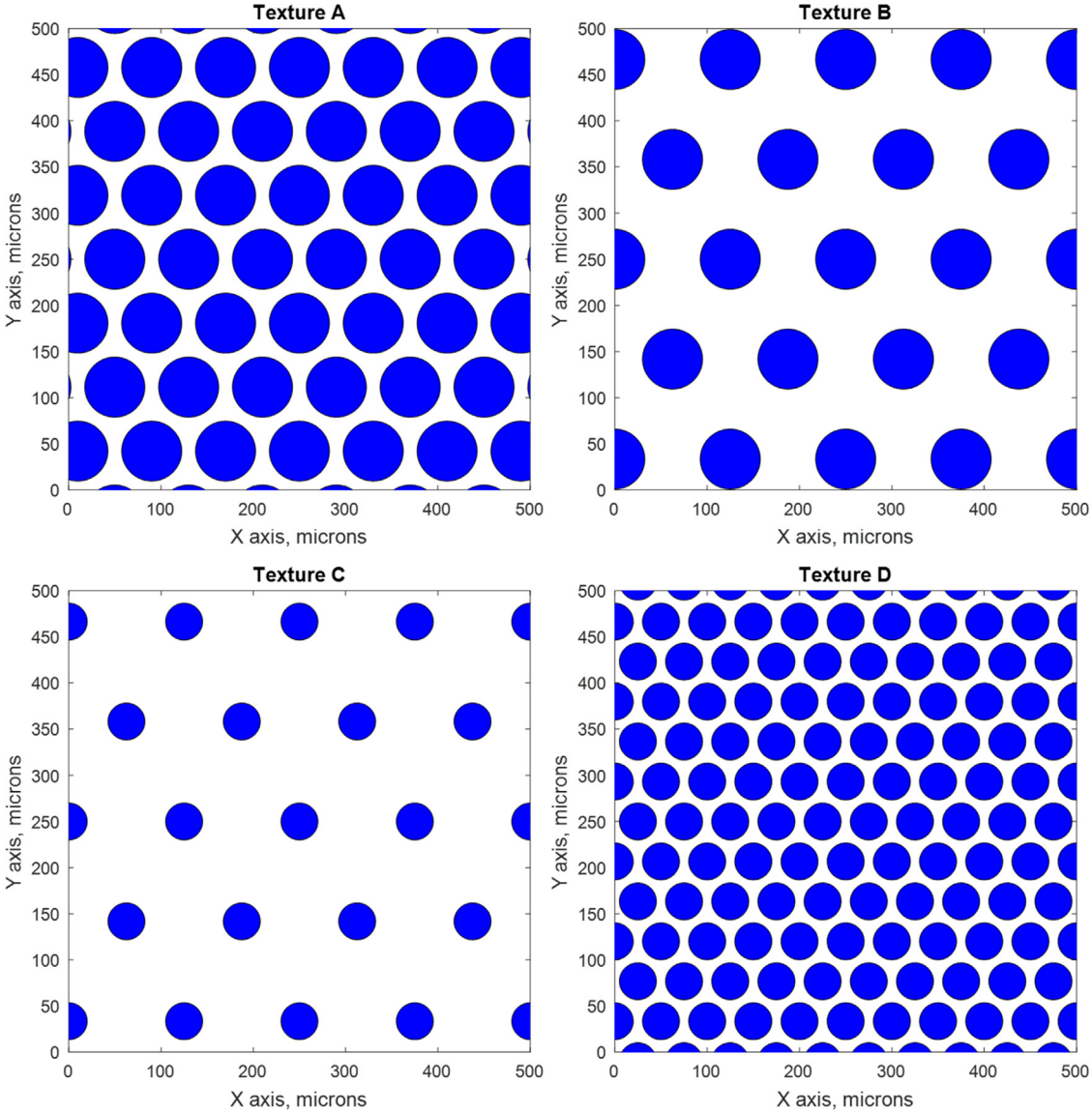

Fig. 8. Schematic of Textures from A to D. White area represents the contact area between the aluminium and the steel surface, whereas blue circles represent craters. (For interpretation of the references to colour in this figure legend, the reader is referred to the web version of this article.).

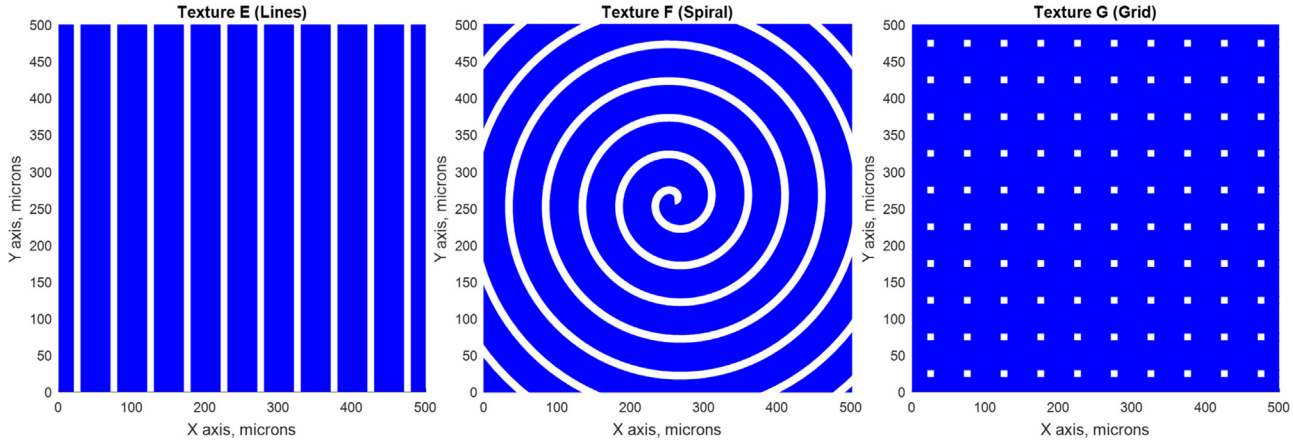

Fig. 9. Schematic of laser-generated textures comprising parallel troughs (Texture E), spiral pattern (Texture F) and a grid of troughs (Texture G). White area represents the contact area between the aluminium and the steel surface, whereas blue area represent the laser-textured area. (For interpretation of the references to colour in this figure legend, the reader is referred to the web version of this article.).

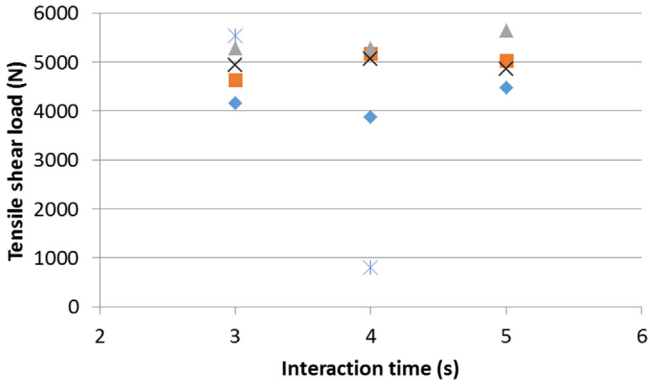

Fig. 10. Tensile shear load as a function of the interaction time for different laser-textured and untextured samples. The results were obtained with PD = 20.1 MW/m^2.

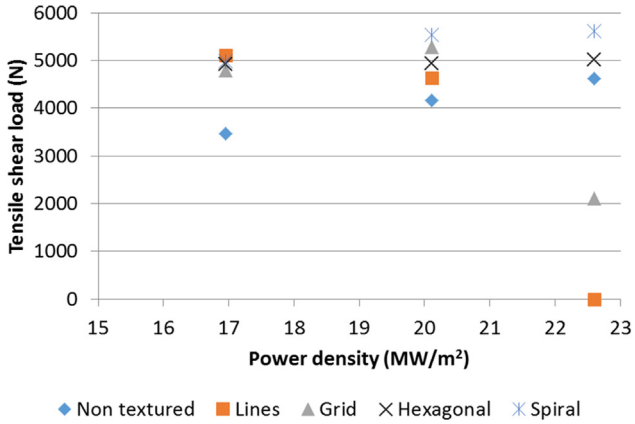

Fig. 11. Tensile shear load as a function of the power density for different laser-textured and untextured samples. The results were obtained with t_i = 3 s.

Within the experimental range, the tensile shear load of the joints was nearly constant with interaction time. This trend was observed for all the tested samples, with the exception of the spiral. When comparing to the untextured joints, which had an average tensile shear load of 4 kN, the joints produced with the textures containing lines, grid and hexagonally-arranged craters showed a higher tensile shear load, with an average value of tensile-shear load of 5 kN. The joint with the highest tensile shear load of >5.5 kN was obtained with the texture G containing the grid pattern using PD = 21.1 MW/m^2 and t_i = 5 s. In contrast, the joint with the lowest tensile shear load (< 1 kN) was obtained with the texture containing the spiral pattern using the interaction time of 4 s. This low tensile shear load is a consequence of the plug failure. Such a failure occurs typically due to the strong reaction between Fe and Al which leads to the mixing of these two metals in the liquid state during the welding process. The plug failure observed in this sample is characteristic of a brittle weld where the weld nugget is made of brittle IMC phases. The high diffusion of Fe into Al and vice-versa, when both metals are mixed in liquid state, enhances the formation of several IMCs at the joint interface, deteriorating the mechanical properties of the joints.

The nearly constant evolution of the tensile shear load with the interaction time for all the textured and untextured samples indicates that the interaction time may not be the most important fundamental laser material interaction parameter in determining the mechanical properties of the joints. The mechanical properties of the joints are dependent on the bonding area and the IMCs formed during the welding process. The fact that within the experimental range the interaction time does not change the maximum tensile shear load of the joints could be either due to the simultaneous growth of the IMCs and the bonding area which in this case are both in balance, or because the interaction time has a small effect on the growth of the IMC and bonding area.

Fig. 11 shows the impact of power density on the tensile shear load of the joints for constant interaction time of 3 s. With 17 MW/m^2 of power density, all samples with textured surfaces have considerably better mechanical properties than the untextured samples. Once again the results show that the patterns are an effective way of improving the mechanical properties of the laser spot welded joints without increasing the process energy. As the power density increased to 20 MW/m^2, all of the textured samples still showed higher tensile shear load than the untextured samples, albeit with a lower difference. For the maximum power density tested, the trend was not verified. Two textures, those containing the grid and lines, showed lower tensile shear load when compared with the untextured samples. This result may be justified by the poor heat conduction from Fe to Al, in particular for the grid pattern where the relative contact area was very small (S = 4%). In general, the presence of craters (air gaps) induces a thermal resistance at the interface between the metals, causing an increase of temperature and consequently melting of the steel. Therefore the temperature of the aluminium is not significantly increased, and the wetting area remains almost unchanged.

The joints produced with the spiral and hexagonal patterns showed higher tensile shear load at higher power densities than the other patterns. This result may be explained by the larger contact area promoted by these two last patterns which allows higher heat conduction and more melting of Al and therefore better wetting of the steel by molten Al.

The textures processed on the steel not only changed the thermal field across the samples, but also changed the wetting behaviour and hence the bonding area between the Al and steel. In the experiment the bonding area, which is also known as the area of the weld nugget, was determined by measuring the fracture surfaces of the steel and aluminium after tensile-shear testing. The fracture surfaces revealed two distinct regions: a dark central region and a bright peripheral region. Here, it should be noted that similar fracture surfaces were observed in resistance spot welded joints between steel and 5052 aluminium alloy by Qiu et al. (Qiu et al., 2009a,b). The authors analysed these regions by SEM and EDS and they found that the peripheral area of the steel contained a significant amount of Al, whereas the dark area in the centre was identified as a mixture of Al and Fe. The results suggested that the fracture propagated through the aluminium located on the peripheral region and through the IMCs located in the central area of the weld. The failure that occurred across the IMCs resulted from the fact that the IMC layer was relatively uniform and thick, and thus more fragile. On the other hand, the IMCs on the peripheral area were discontinuous and thin, and therefore it was believed that the failure occurred on the aluminium.

Similar analysis of the fracture surfaces was performed in the presented work. Fig. 12 shows the optical micrographs of selected areas on the steel surface after the tensile-shear test.

The left column of Fig. 12 presents the regions outside the weld nuggets which were not wetted by the molten aluminium. These micrographs reveal different textures that were generated on the surface of the steel before welding. The middle column of Fig. 12 presents the peripheral region of the weld nuggets, showing the impact of the laser-generated patterns on the flow of the molten aluminium during the welding process. These micrographs show clearly that the molten aluminium penetrates into the microchannels, confirming that the laser-generated patterns play an important role in the formation of the bonding area between Fe

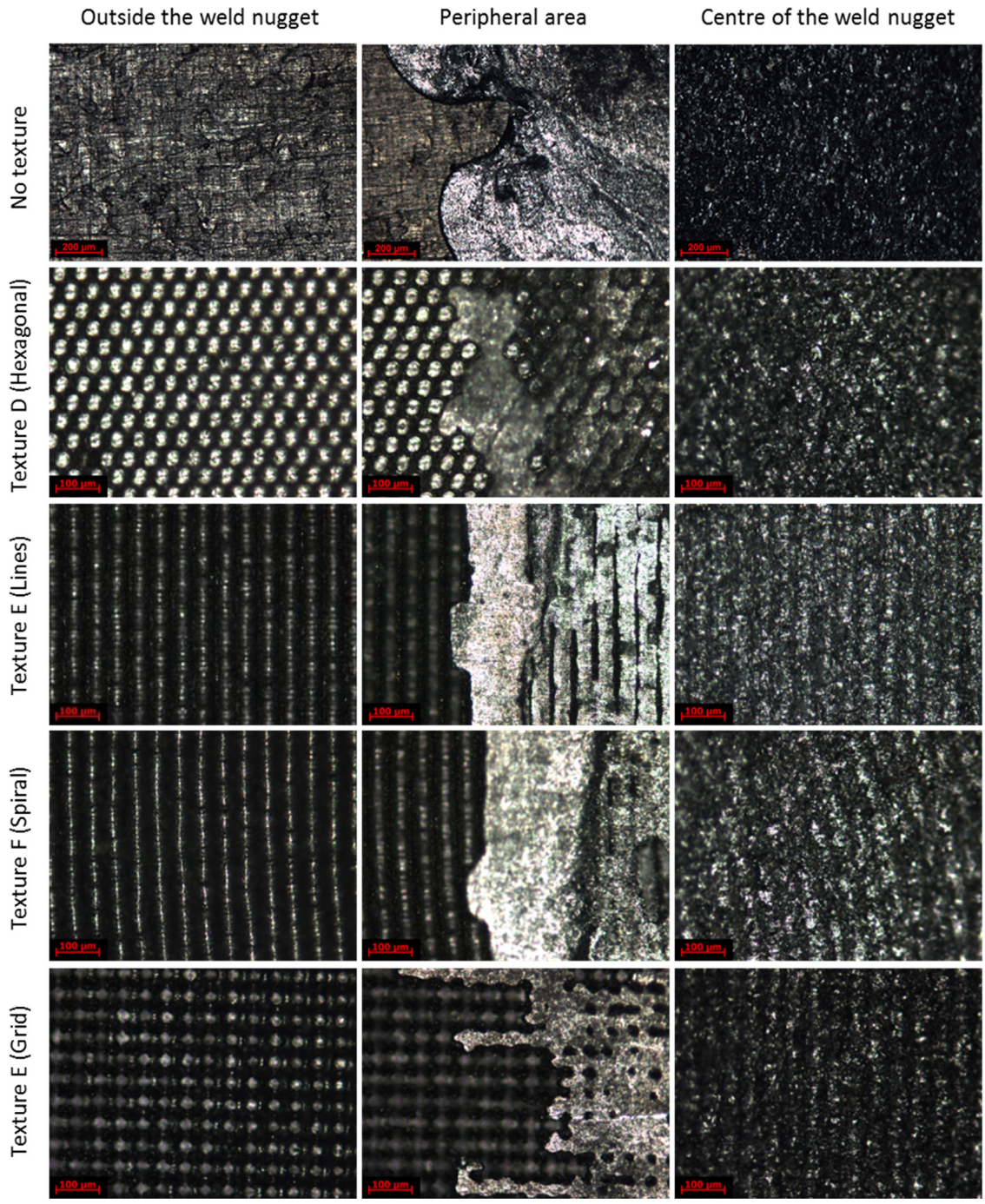

Fig. 12. Micrographs showing the fracture surface on the steel side after tensile-shear testing. The samples were produced using PD = 20.1 MW/m^2 and t_i = 3 s.

and Al. In the case of the textures containing the spiral and parallel lines, the direction of the flow of the molten aluminium is constrained by the orientation of the micro-channels, while the grid and hexagonal patterns permit the molten aluminium to be spread in more than one direction. The steel surface of the untextured sample was wetted by the molten aluminium, but the flow direction did not follow any preferential direction.

The cross sections of the weld nuggets are shown in Fig. 13. These fractographs show the IMC layer that was formed in the central region of the weld nugget, which proves that the textures were successfully wet by the molten aluminium, in particular those comprising the grid, spiral and hexagonally-arranged craters, and that the bonding area was increased. The fractographs also indicate that the growth of the IMC layer was influenced by the texture geometry. This can be clearly observed in Fig. 13c)–e) where the IMC was formed inside the laser-generated micro-channels. For the untextured steel, the IMC layer was thin but it was spread continuously across the metal surface, as can be seen in Fig. 13a).

The bonding area of all joints was measured to permit a quantitative analysis of the effect of the patterns and welding parameters on the weld nugget. The bonding area was measured from macrographs taken on the Fe side at fractrographic plane. The total area of the weld nuggets resultant from the welding process with variable

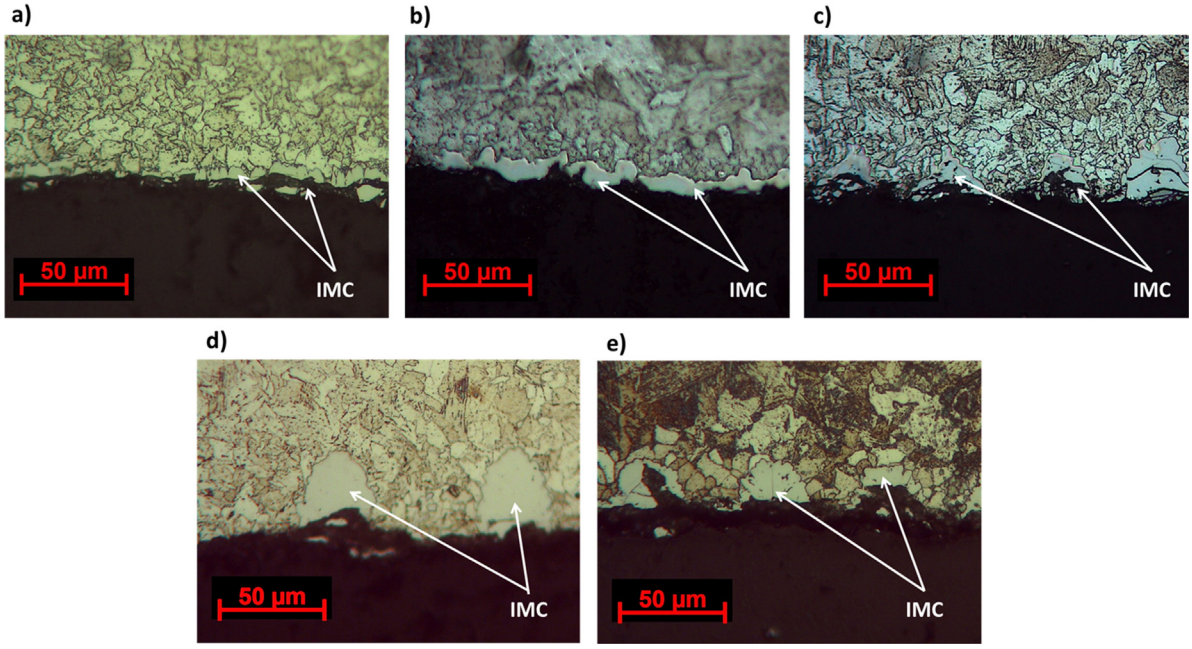

Fig. 13. Cross-sectional fractography of the joint showing only the steel plate for: a) untextured and laser-textured steel with b) parallel lines, c) grid, d) hexagonal-arranged craters and e) spiral patterns.

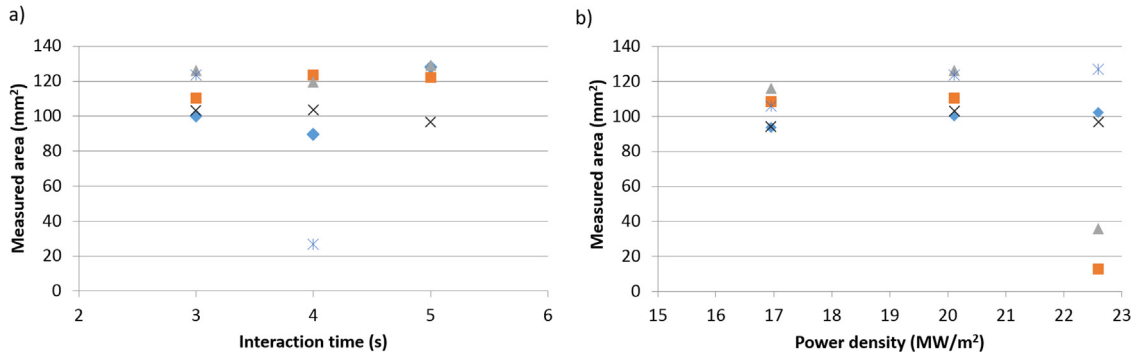

Fig. 14. Total bonding area (central + peripheral) for the welded samples and plotted for the increasing: a) interaction time and b) power density.

interaction time and power density is presented in Fig. 14a) and b), respectively.

The textured joints had similar or even a larger weld nugget area than the untextured joints for the interaction times of 3 s and 4 s. For the interaction time of 5 s, however, the bonding area of the untextured joints was larger than that of the textured joints. A similar trend was observed in Fig. 14b. For power densities up to 20 MW/m^2, all the textured joints had weld nuggets with equal or even larger total areas in comparison with the untextured joints. This shows that for identical welding parameters the introduction of a texture on the steel surface can improve the wettability of the metal, making the weld nuggets larger. For power densities of 22.7 MW/m^2, however, the surfaces containing the lines, grid and spiral patterns induced a smaller bonding area than the untextured surface. This explains the low tensile shear load of the joints produced with the grid and line textures (see Fig. 11).

Fig. 15 shows the correlation between the tensile shear strength (which was calculated for each sample) and (a) the interaction time (t_i) and (b) the power density (PD).

With the increase in power density, all of the textured samples have higher mechanical properties than the untextured samples. The only exceptions were the joints obtained with the spiral and lines patterns at PD = 22.7 MW/cm^2.

The highest tensile shear strength of approximately 60 MPa was obtained with the sample containing the grid pattern at PD = 22.7 MW/cm^2. This sample had a maximum shear load of 2 kN, but the wetting area was very small, due to the high power density and the uncontrolled mixing of both metals during welding. Even though this resulted in the highest strength obtained for all of the tested samples, this was not the sample with the highest load. This shows once again the non-linear relationship between the tensile strength and the bonding area when the intermetallic compounds are present.

Comparing the results obtained in this work with the results available in the literature, one can observe an improvement on the tensile shear load of the Fe-Al joints. For example, the maximum tensile-shear load of 5 kN was obtained by resistance spot welding (Qiu et al., 2009a,b), whilst the results reported in the present work had a maximum tensile-shear load of 5.6 kN.

Based on the results presented in this section, it can be concluded that the laser-generated patterns change the wetting of the steel surface by the molten aluminium, often improving the

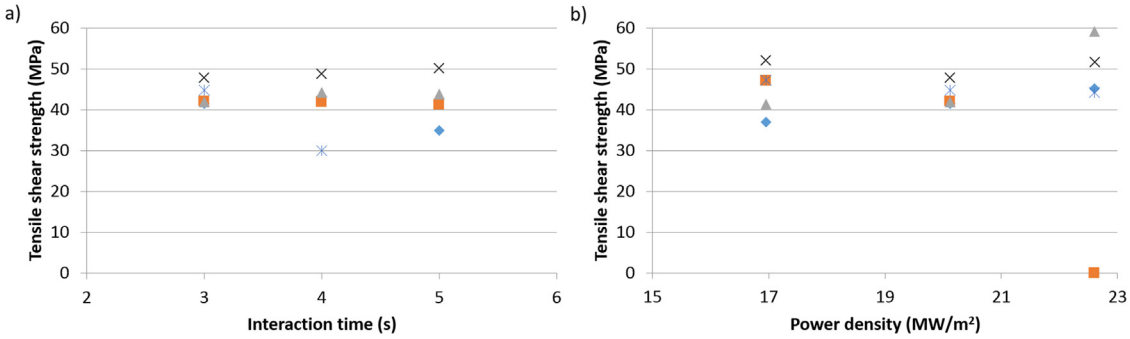

Fig. 15. Tensile shear strength calculated using (central + peripheral) area for different: a) interaction times and b) power densities.

mechanical strength of the joints. They also determine the dimension and quality of the bonding area because the patterns allow the molten aluminium to flow into micro-channels on the steel surface, interlocking the two metals together. The laser-generated textures also determine the amount of heat that is transferred to the aluminium. Therefore, the results show that if one wants to increase the ultimate tensile shear load of the Fe-Al joints and use a wider range of welding parameters to produce the joints then the best texture to choose is the hexagonal pattern. However, the joints produced with the hexagonal pattern did not have the maximum tensile-shear load nor the largest bonding area but these features were constant within the range of the experimental parameters. On the other hand, in order to produce Fe-Al joints with a tensile shear load of > 5.5 kN, the best textures to choose are the grid and spiral patterns. The load of > 5.5 kN can be obtained with the grid pattern when PD = 20.1 MW/m^2 and t_i = 5 s, whereas with the spiral pattern when PD = 22.7 MW/m^2 and t_i = 3 s.

4. Conclusions

The conclusions presented in this paper are based on preliminary tests performed to investigate the influence of different texture patterns on the mechanical performance of dissimilar metal laser spot welded joints. Various textures containing craters arranged in different patterns: hexagonal, parallel lines, grids and spirals were investigated in order to determine the impact of the texture on the maximum tensile-shear load of the joints. The textures were tested with different laser energy levels, by changing either the power density or interaction time, during laser spot welding to understand how the textures would affect the thermal field in the joined metals as well as the wetting of the steel surface by the molten aluminium.

The main conclusions of this preliminary study are as follows:

- Defect free Fe-Al joints were produced by laser spot welding using laser-textured steel;
- Compared to the untextured samples, the laser-textured surfaces enabled the joints to increase the maximum tensile-shear load by approximately 25%;
- The maximum tensile-shear load obtained in this work was equivalent to that reported in the literature for joints between Al–Al (Qiu et al., 2009a,b);
- The joints welded with the hexagonal texture had maximum tensile-shear load with 40 μm diameter craters, 30 μm deep, separated by a distance of 50 μm;
- Textures comprising lines, grid and spiral patterns had a smaller working envelope than the untextured samples;
- The results suggest that the maximum tensile-shear load was improved not only due to an increase in the bonding area, but also due to the quality and uniformity of the weld nuggets.

Acknowledgements

The research covered in this paper was funded by the Engineering and Physical Sciences Research Council (EPSRC), the Centre for Innovative Manufacturing in Laser-based Production Processes (Grant No.: EP/K030884/1). Additional support was provided by Alicona and SPI Lasers UK Ltd.. Data underlying this study can be accessed through the Cranfield University repository at: http://dx.doi.org/10.17862/cranfield.rd.4205307.

References

Assuncao, E., Williams, S., Yapp, D., 2012. Interaction time and beam diameter effects on the conduction mode limit. Opt. Lasers Eng. 50, 823–828, http://dx.doi.org/10.1016/j.optlaseng.2012.02.001.

Borrisutthekul, R., Yachi, T., Miyashita, Y., Mutoh, Y., 2007. Suppression of intermetallic reaction layer formation by controlling heat flow in dissimilar joining of steel and aluminum alloy. Mater. Sci. Eng. A 467, 108–113, http://dx.doi.org/10.1016/j.msea.2007.03.049.

Cao, R., Huang, Q., Chen, J.H., Wang, P.C., 2014. Cold metal transfer spot plug welding of AA6061-T6-to-galvanized steel for automotive applications. J. Alloys Compd. 585, 622–632, http://dx.doi.org/10.1016/j.jallcom.2013.09.197.

Chen, Y.C., Gholinia, a., Prangnell, P.B., 2012. Interface structure and bonding in abrasion circle friction stir spot welding: a novel approach for rapid welding aluminium alloy to steel automotive sheet. Mater. Chem. Phys. 134, 459–463, http://dx.doi.org/10.1016/j.matchemphys.2012.03.017.

Church, G., 2015. Laser Systems Europe. Keep. Cars Light Their Wheel. Issue 28, URL http://www.lasersystemseurope.com/feature/keeping-cars-light-their-wheels (Accessed 20 January 2016).

Dunn, A., Carstensen, J.V., Wlodarczyk, K.L., Hansen, E.B., Gabzdyl, J., Harrison, P.M., Shephard, J.D., Hand, D.P., 2014. Nanosecond laser texturing for high friction applications. Opt. Lasers Eng. 62, 9–16, http://dx.doi.org/10.1016/j.optlaseng.2014.05.003.

Dunn, A., Wlodarczyk, K.L., Carstensen, J.V., Hansen, E.B., Gabzdyl, J., Harrison, P.M., Shephard, J.D., Hand, D.P., 2015. Laser surface texturing for high friction contacts. Appl. Surf. Sci. 357, 2313–2319, http://dx.doi.org/10.1016/j.apsusc.2015.09.233.

Havrilla, D., 2014. Laser joining of aluminum poised to grow as cars lose weight. Ind. laser Solut. Manuf., URL http://www.industrial-lasers.com/articles/print/volume-29/issue-3/features/laser-joining-of-aluminum-poised-to-grow-as-cars-lose-weight.html (Accessed 20 March 2016).

Lesemann, M., Sahr, C., Hart, S., Taylor, R., 2008. SuperLIGHT-CAR—the multi-material car body, in: proceedings of the 7th LS-DYNA anwenderforum. Bamberg, 1–10.

Martinsen, K., Hu, S.J., Carlson, B.E., 2015. Joining of dissimilar materials. CIRP Ann.—Manuf. Technol. 64, 679–699, http://dx.doi.org/10.1016/j.cirp.2015.05.006.

Meco, S., Pardal, G., Ganguly, S., Williams, S., McPherson, N., 2015. Application of laser in seam welding of dissimilar steel to aluminium joints for thick structural components. Opt. Lasers Eng. 67, 22–30, http://dx.doi.org/10.1016/j.optlaseng.2014.10.006.

Oikawa, H., Saitoh, T., 1999. Resistance spot welding of steel and aluminium sheet using insert metal. Weld. Int. 13, 349–359, http://dx.doi.org/10.1080/09507119909446510.

Pardal, G., Meco, S., Ganguly, S., Williams, S., Prangnell, P., 2014. Dissimilar metal laser spot joining of steel to aluminium in conduction mode. Int. J. Adv. Manuf. Technol. 73, 365–373, http://dx.doi.org/10.1007/s00170-014-5802-y.

Qiu, R., Iwamoto, C., Satonaka, S., 2009a. Interfacial microstructure and strength of steel/aluminum alloy joints welded by resistance spot welding with cover plate. J. Mater. Process. Technol. 209, 4186–4193, http://dx.doi.org/10.1016/j.jmatprotec.2008.11.003.

Qiu, R., Iwamoto, C., Satonaka, S., 2009b. The influence of reaction layer on the strength of aluminum/steel joint welded by resistance spot welding. Mater. Charact. 60, 156–159, http://dx.doi.org/10.1016/j.matchar.2008.07.005.

Vilhena, L.M., Sedlaček, M., Podgornik, B., Vižintin, J., Babnik, A., Možina, J., 2009. Surface texturing by pulsed Nd:YAG laser. Tribol. Int. 42, 1496–1504, http://dx.doi.org/10.1016/j.triboint.2009.06.003.

Williams, S., Suder, W., 2011. Use of fundamental laser material interaction parameters in laser welding. In: In: Conference on Lasers and Electro-Optics (CLEO). IEEE, Baltimore, MD, pp. 1–2.

Zhang, W.H., Qiu, X.M., Sun, D.Q., Han, L.J., 2011. Effects of resistance spot welding parameters on microstructures and mechanical properties of dissimilar material joints of galvanised high strength steel and aluminium alloy. Sci. Technol. Weld. Join. 16, 153–161, http://dx.doi.org/10.1179/1362171810Y.;1;0000000009.

2017-03

Laser spot welding of laser textured steel to aluminium

Pardal, Goncalo

Elsevier

Pardal G, Meco S, Dunn A, et al., Laser spot welding of laser textured steel to aluminium.
þÿ J o u r n a l o f M a t e r i a l s P r o c e s s i n g T e c h n o l o g y , V o l u m e 2 4 1 , M a r c h 2 0 1 7 , p p
http://dx.doi.org/10.1016/j.jmatprotec.2016.10.025